Materials Science and Engineering A361 (2003) 350–357

MATERIALS SCIENCE & ENGINEERING A

www.elsevier.com/locate/msea

Modeling of resistance curve of high-angle grain boundary in Fe–3 wt.% Si alloy

Y. Qiao*

Department of Civil Engineering, University of Akron, ASEC 210H, 244 Summer St., Akron, OH 44325-3905, USA

Received 15 May 2003; received in revised form 28 June 2003

Abstract

When a propagating cleavage front encounters a high-angle grain boundary it first penetrates through the grain boundary stably. With increasing penetration depth the resistance of the grain boundary rises, resulting in the well-known *R*-curve. When the balance between the rates of the energy release rate and the grain boundary resistance is reached, the crack advance becomes unstable and the grain boundary is broken through. In this paper, this process is analyzed quantitatively based on the experimental observations of the cleavage cracking in Fe–3 wt.% Si bicrystals. The effects of the crystal misorientation, the crack length, and the crack front profile are discussed.

Keywords: Cleavage; Grain boundary; Resistance curve; Fe–3 wt.% Si alloy; Fracture toughness

1. Introduction

In intrinsically brittle materials including many BCC metals and alloys, the fracture mode is cleavage at lower shelf of ductile-to-brittle (DB) transition region [1–3]. When the cleavage crack propagates across a field of grains, both of the crack-tip dislocation emission and the formation of the cleavage facets are interrupted by the grain boundaries. In the cleavage cracking across a high-angle grain boundary the crack front must be geometrically necessarily branched, which, together with the separation of the grain boundary between the break-through points, results in the additional fracture work. This toughening effect can lower the DB transition temperature considerably and has been noticed for decades in experiments where the behavior of the grain-sized microcracks was dominant [4–6].

The microstructure dependence of the grain boundary resistance to cleavage crack advance was first studied by Gell and Smith [7] in hydrogen charged Fe–3% Si polycrystals. By measuring the probability for the microcracks to break through the grain boundaries with different crystallographic misorientations it was concluded that the rotation angle had little influence on the grain boundary toughness while the effect of the twist misorientation was significant. The break-through event was modeled as an arrest–renucleation process, with the renucleation of the new cleavage facets in adjacent grains being the critical step. More detailed analysis of the features on the separated grain boundaries showed that the break-through modes could actually be classified into four types [8].

The role of the grain boundaries in fracture was often related to their influence on the competition between the plastic shielding and the cleavage cracking [9]. In a theoretical study of the cleavage fracture after extended plastic deformation, McClintock [10] argued that the factor dominating the overall fracture resistance was the separation of the grain boundaries, which was modeled as pure shear combined with coplanar shear fracture. The work associated with the cleavage cracking insides grains was ignored.

Although the results of these models fit quite well with a substantial subset of the experimental observations, they shed little light on the micromechanisms of the crack–boundary interaction. In the present study, based on the experimental results of the grain boundary toughness of Fe–3 wt.% Si bicrystals [11], the resistance curve of the grain boundary was analyzed in context of linear elastic fracture mechanics. The effects of the work of separation of the grain boundary, the crack front profile, as well as the crack length were discussed in considerable detail.

* Tel.: +1-330-972-2426; fax: +1-330-972-6020.
E-mail address: yqiao@uakron.edu (Y. Qiao).

0921-5093/$ – see front matter © 2003 Elsevier B.V. All rights reserved.
doi:10.1016/S0921-5093(03)00534-3

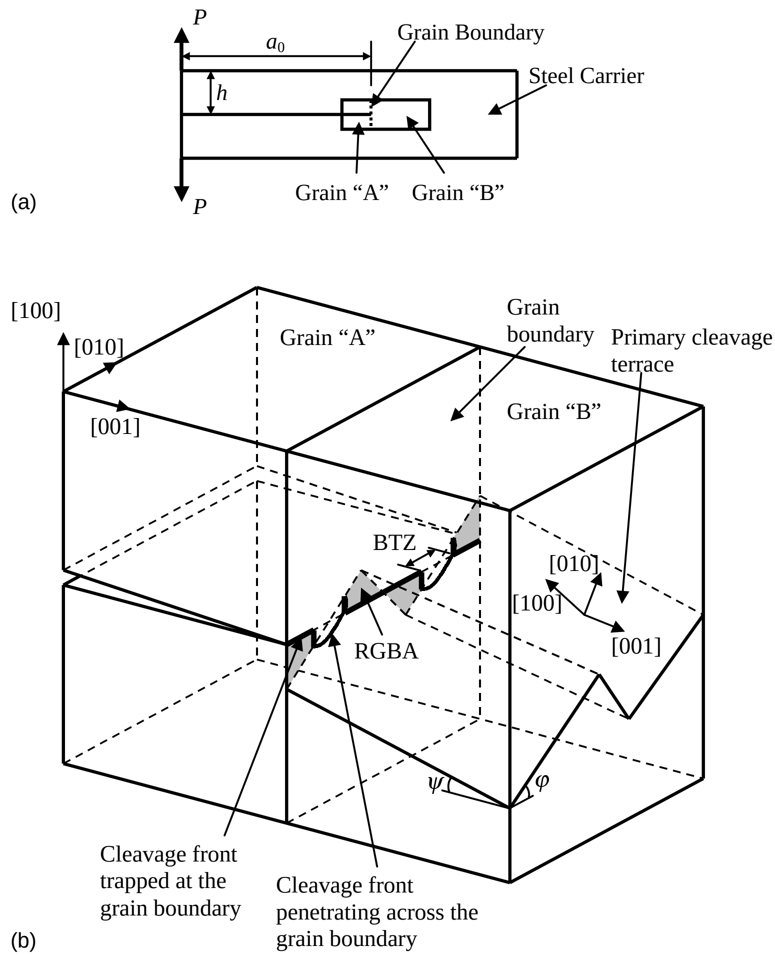

Fig. 1. Schematic diagrams of: (a) the double cantilever beam specimen of the Fe–3 wt.% Si bicrystal and (b) the crystallographic orientation of the bicrystal.

2. Cleavage cracking across high-angle grain boundaries in Fe–3 wt.% Si bicrystals

In order to quantify the toughening effect of high-angle grain boundaries, Qiao and Argon [11] performed the grain boundary toughness measurement experiment in 17 Fe–3 wt.% Si bicrysals. As depicted in Fig. 1(a) the pre-cracked bicrystal was electron-beam welded into a steel carrier to fabricate the double-cantilever beam (DCB) specimen. In all the bicrystals, grain "A" was of the same crystallographic orientation with the (1 0 0) cleavage plane parallel to the median plane of the specimen, and the orientation of grain "B" was random (see Fig. 1(b)). The grain boundary toughness, K_{ICGB}, was obtained by measuring the critical load P for the crack to break though the grain boundary. The details of the experimental procedure are discussed elsewhere [11].

Fig. 2 is a SEM fractograph showing the break-through process across the grain boundary. The cleavage front first penetrated through the grain boundary in a number of break-through zones (BTZ) distributed along the front quasi-periodically, with the rest of the front trapped locally by the recalcitrant grain boundary areas (RGBA) between the BTZ. The area of RGBA was related to the width and the spacing of BTZ, as well as the twist misorientation. Observation of the profile of the river markings inside BTZ indicated that the cleavage front advance was of fanning-out nature (see Fig. 3). With increasing stress intensity at the crack tip, in BTZ, the front penetrated into grain "B" deeper and deeper and the width of BTZ increased continuously, as depicted in Fig. 4. When the critical penetration depth was reached, RGBZ was separated through mixed mode fracture triggered by the "preparatory" plastic shear deformation, and the crack overcame the resistance of the grain boundary. Fig. 5 is the SEM micrograph of a separated RGBA showing signs of both fracture-type separation and plastic shearing. In Fig. 2, it can be seen that after entering in grain "B" the cleavage front branched into a number of terraces parallel to the (1 0 0) plane.

By considering the contributions to the fracture work of both RGBA and the cleavage facets, Qiao and Argon

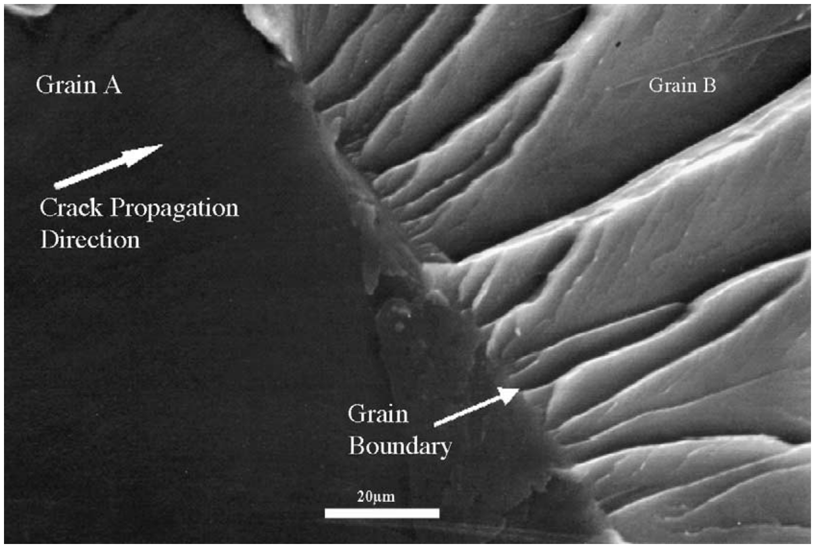

Fig. 2. SEM fractography of the break-through process of the cleavage crack across a high-angle grain boundary.

suggested a simply expression for K_{ICGB} [11]

$$\left(\frac{K_{\mathrm{ICGB}}}{K_{\mathrm{ICSC}}}\right)^2 = C\frac{\sin\varphi\cos\varphi}{\cos\psi} + \frac{1}{(\cos\psi)^2}(\sin\varphi + \cos\varphi) \quad (1)$$

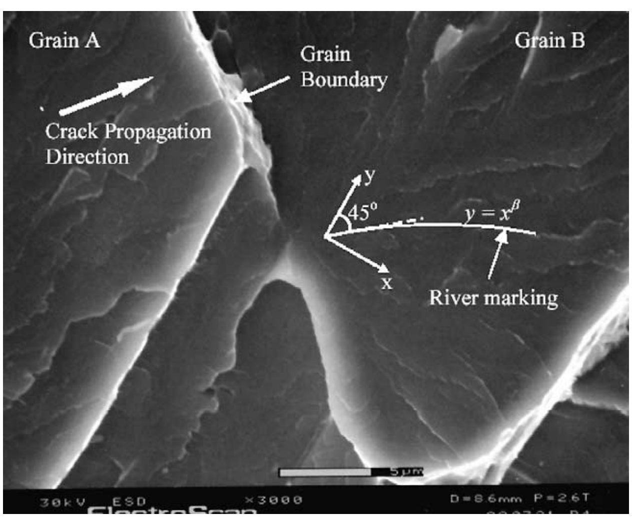

Fig. 3. SEM micrograph of a break-through zone (BTZ).

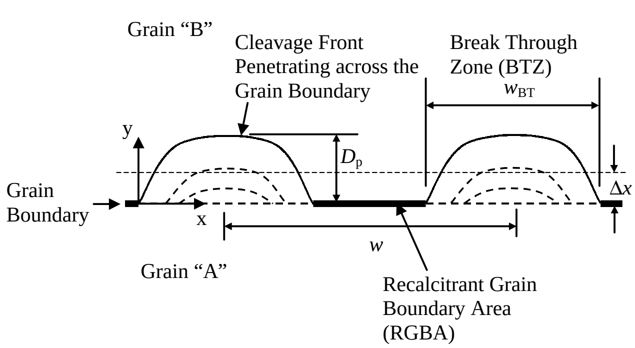

Fig. 4. Cleavage front penetrating across a high-angle grain boundary.

where K_{ICSC} is the critical stress intensity factor of the single crystal; φ and ψ are the twist and the tilt misorientations, respectively; and $C = \tilde{\beta}kw/4G_{\mathrm{ICSC}}$ is a material constant, with $\tilde{\beta}$ being the ratio of the shear distance of the grain boundary to the effective penetration depth Δx, k being the effective grain boundary shear strength, and w being the average spacing between BTZ. The contribution of the work of separation of RGBA was captured by the first term at RHS of Eq. (1), and the second term reflected the fracture work associated with the cleavage facets in grain "B". In this model, the role of the grain boundary is somewhat similar to that of the ligaments behind the cleavage front that fail via tearing [12,13]. Note that, although the results of Eq. (1) fit with the experimental data quite well, since the calculation of K_{ICGB} was based on the area average of the fracture work, the evolution of the cleavage front profile could not be accounted for. Furthermore, the assumption that the shear distance was proportional to the penetration depth was quite empirical.

As discussed above, even when the overall stress intensity was below G_{ICGB}, the crack front could start to penetrate through the grain boundary in BTZ, resulting in the effective crack growth Δx. As depicted in Fig. 3, Δx can be estimated through the position of the centroids of the cleavage facets in grain "B". The effective crack length increases gradually with the stress intensity, i.e. the more the crack advances, the higher the resistance of the grain boundary, which can be described by the well-known R-curve depicted in Fig. 6. With the constant external load per unit thickness, P, the energy release rate G increases with the crack length a. When $P = P_1$ is relatively low, the energy release rate of the crack with the initial length of a_0 is below G_{in}, the critical value of the onset of the crack growth. The crack length remains a_0 until P is increased to P_2 when the crack starts to grow. Since the resistance to crack advance rises more rapidly than the energy release rate, the crack will be stopped immediately,

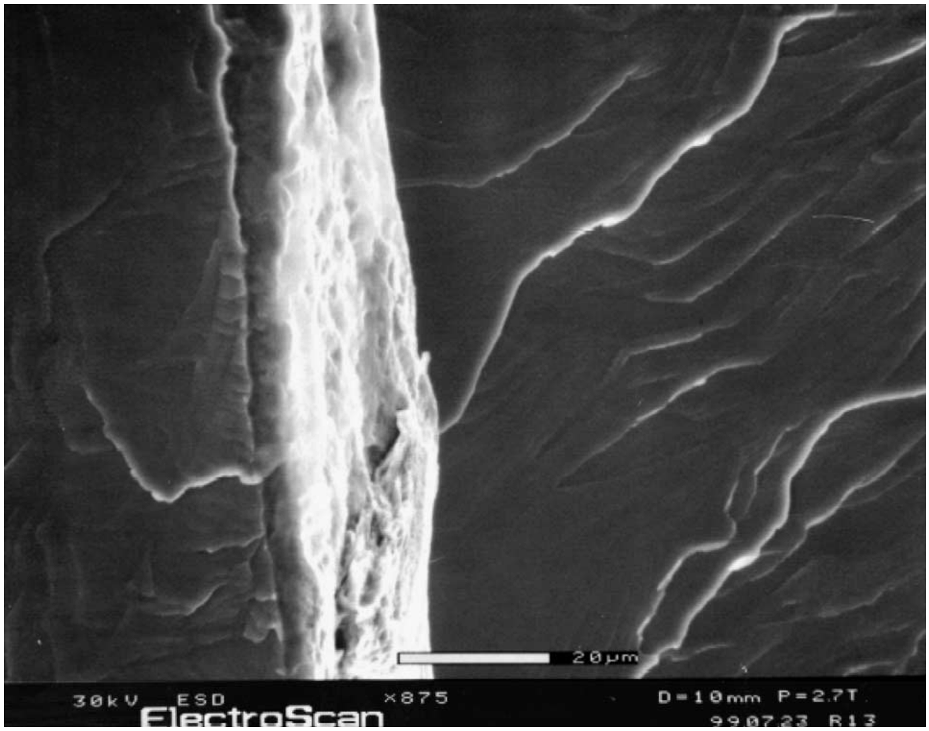

Fig. 5. SEM micrograph of a grain boundary showing signs of both fracture-type separation and plastic shearing.

i.e. the crack growth is stable. With increasing external load, the crack grows gradually until the crack length reaches a_{cr}, where

$$\frac{\partial G}{\partial a} = \frac{\partial R}{\partial a} \tag{2}$$

with R being the resistance to cracking. When the crack length is larger than a_{cr}, the resistance increases slower than the energy release rate. Consequently the crack propagation becomes unstable and the final failure occurs. Since $\partial G/\partial a$ is often a function of a, the critical energy release rate of the unstable crack advance and the critical crack length a_{cr} are often related to the initial crack length.

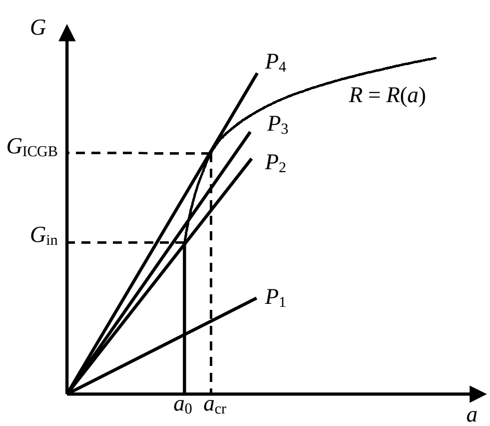

Fig. 6. Schematic diagram of R-curve.

In the fracture experiment of the DCB specimens of Fe–3 wt.% Si bicrystals, G_{in} could not be obtained. The measured toughness of the high-angle grain boundaries, K_{ICGB}, was actually the critical value of the unstable crack advance. In the following discussion, we will study this phenomenon in context of R-curve analysis to take account for the crack–boundary interaction.

3. Resistance curve of high-angle grain boundary

The resistance to crack advance across the grain boundary can be studied through the fracture work associated with the effective crack growth distance Δx. Assume that with increasing penetration depth, the width of BTZ, w_{BT}, increases as

$$\frac{w_{BT}}{w} = \alpha \left(\frac{\Delta x}{w}\right)^{\beta}. \tag{3}$$

If the cleavage front is elliptical, the value of β can be estimated through the profile of the river markings that are normal to the verge of propagating. The coordinate system should be taken as shown in Fig. 3 with the line $y = x$ parallel to the initial tangent of the river marking accounting for the fact that if $w_{BT}/\Delta x$ ratio is constant the river marking should be straight. It was found that $y = x^{0.6}$ fit with the river markings quite well. Thus, in the following calculation, β is taken as 0.6.

The fracture work W consists of the work of separation of the grain boundary in BTZ, W_{GB}, and the work associated with the cleavage facets in grain “B”:

$$W = W_{GB} + G_{ICB}\,\Delta x \quad (4)$$

with G_{ICB} being the critical energy release rate of grain “B”. Note that W_{GB} is caused by the plastic shear deformation along the grain boundary between the cleavage facets in grains “A” and “B” [11]

$$W_{GB} = \frac{1}{w}[kw_{BT}^2(\varepsilon_f h_{GB})]\frac{\sin\varphi\cos\varphi}{4} \quad (5)$$

where $\varepsilon_f h_{GB}$ is the “preparatory” shear distance at which the fracture-type separation occurs, with ε_f being the critical shear strain and h_{GB} being the height of the grain boundary in BTZ, which can be stated as:

$$\varepsilon_f = \frac{k}{\mu} \quad (6)$$

$$h_{GB} = w_{BT}\cos\varphi\sin\frac{\varphi}{2} \quad (7)$$

with μ being the shear modulus. Substituting Eqs. (5)–(7) into Eq. (4) gives the resistance curve

$$R = \frac{W}{\Delta x} = k^* w(\sin\varphi\cos\varphi)^2\tilde{x}^m + G_{ICB} \quad (8)$$

where $\tilde{x} = \Delta x/w$, $k^* = \alpha^3k^2/8\mu$, and $m = 3\beta - 1$.

In the DCB specimen shown in Fig. 1(a), if the height of the DCB arm, h, is much smaller than the initial crack length, a_0, and the free edge effect is negligible, the energy release rate can be calculated through basic beam theory

$$G = \frac{12P^2a^2}{Eh^3}\cdot \quad (9)$$

Thus, the critical condition of the unstable cleavage crack advance across the grain boundary, Eq. (2), can be rewritten as:

$$\frac{24P^2a_{cr}}{Eh^3} = k^* m(\sin\varphi\cos\varphi)^2\tilde{x}^{m-1} \quad (10)$$

where $a_{cr} = a_0 + \tilde{x}w$. Substitution of Eq. (9) into Eq. (10) gives

$$\frac{2G_{ICGB}}{a_{cr}} = k^* m(\sin\varphi\cos\varphi)^2\tilde{x}^{m-1}, \quad (11)$$

which leads to

$$\tilde{x} = \left[\frac{2G_{ICGB}}{a_{cr}mk^*}\frac{1}{(\sin\varphi\cos\varphi)^2}\right]^{1/(m-1)}. \quad (12)$$

Note that $G = R$ when the crack advances. Hence, we have

$$G_{ICGB} = k^* w(\sin\varphi\cos\varphi)^2\tilde{x}^m + G_{ICB}\cdot \quad (13)$$

Combination of Eqs. (12) and (13) gives the solution of G_{ICGB}.

Through Fig. 3, it can be seen that the peak penetration depth D_p of the cleavage front across the grain boundary was below 2–3 μm. Thus, in most of the engineering materials the initial crack length a_0 is much larger than Δx if the crack is longer than the grain size, i.e. $a_{cr} \approx a_0$. Under this condition, the combination of Eqs. (12) and (13) can be simplified as

$$\tilde{K}^{2/(1-m)} - \tilde{K}^{2m/(1-m)} = \hat{k} \quad (14)$$

where $\tilde{K} = K_{ICGB}/K_{ICB} = (G_{ICGB}/G_{ICB})^{1/2}$ and $\hat{k} = [(m/2)^m(a_0/w)^m(\sin\varphi\cos\varphi)^{2m}(k^*w/G_{ICB})]^{1/(1-m)}$. By considering the cleavage terraces in grain “B”, G_{ICB} can be stated as:

$$G_{ICB} = \frac{G_{ICSC}}{\cos\psi}(\sin\varphi + \cos\varphi)\cdot \quad (15)$$

Consequently, we have

$$\tilde{K} = \frac{K_{ICGB}}{K_{ICSC}}\sqrt{\frac{\cos\psi}{\sin\varphi + \cos\varphi}} \quad (16)$$

and

$$\hat{k} = \left[\left(\frac{m}{2}\right)^m\frac{(\sin\varphi\cos\varphi)^{2m}\cos\psi}{\sin\varphi + \cos\varphi}\left(\frac{a_0}{w}\right)^m\frac{\alpha^3k^2w}{8\mu G_{ICSC}}\right]^{1/(1-m)}. \quad (17)$$

Through Eqs. (14), (16) and (17), the grain boundary toughness can be calculated quite conveniently. The solution of Eq. (14) is shown in Fig. 7. It can be seen that $\tilde{K}$ increases with $\hat{k}$, and the relationship between them can be regressed as

$$\tilde{K} = 1 + 0.25\hat{k}^{0.21}\cdot \quad (18)$$

Substitution of Eqs. (16) and (17) into Eq. (18) gives

$$\hat{K} = \left[1 + 0.12k_0\left(\frac{\sin^2\varphi\cos^2\varphi\cos\psi}{\sin\varphi + \cos\varphi}\right)^{1.05}\right] \times \sqrt{\frac{\sin\varphi + \cos\varphi}{\cos\psi}} \quad (19)$$

where $\hat{K} = K_{ICGB}/K_{ICSC}$ and $k_0 = [(a_0/w)^m(\alpha^3/8)(k/\mu)(kw/G_{ICSC})]^{1.05}$. Equation (19) indicates that the grain boundary toughness is dominated by the twist and tilt misorientation angles, as well as the parameter k_0 collecting together with both some well known factors, such as G_{ICSC}, w, μ, and a_0, and some ill defined factors, such as α and k.

4. Discussion

If we take k_0 as 15.2, the results of Eq. (19) fit very well with the experimental data obtained in the Fe–3 wt.% Si bicrystal experiment [11], as shown in Fig. 8 and Table 1. In the experiment, the work of separation of the single crystal was measured to be about 850 J/m, the spacing between BTZ was in the range of 2–4 μm, the yield strain was about 0.1%, and the initial crack length was about 60 mm. The tensile strength Y of the Fe–3% Si crystals at the experimental

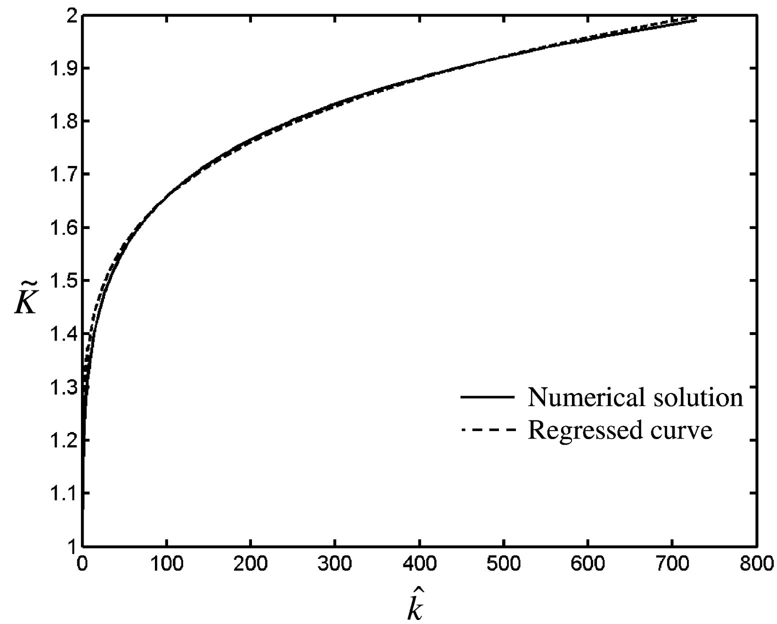

Fig. 7. The relationship between $\tilde{K}$ and $\hat{k}$.

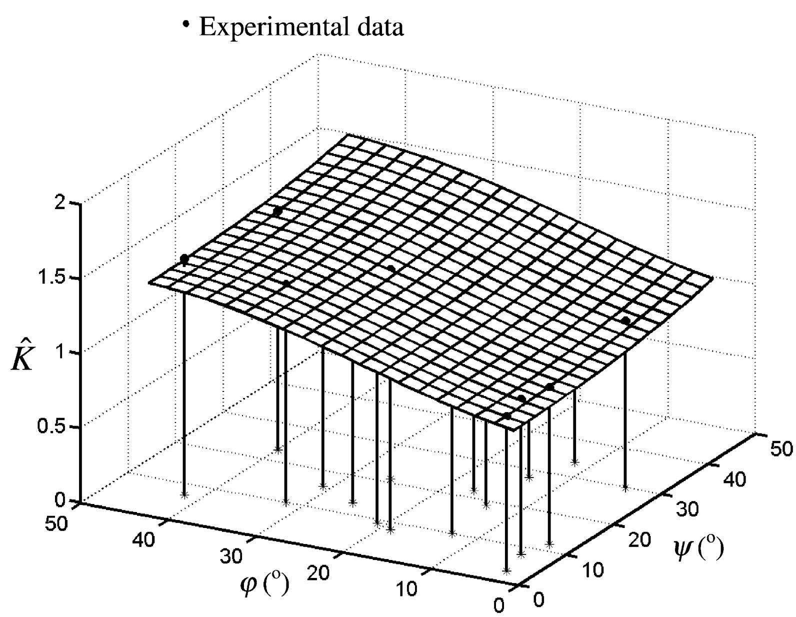

Fig. 8. The grain boundary toughness as function of the crystal misorientation.

Table 1
Comparison of the experimental data [11] and the theoretical results of the grain boundary toughness of Fe–3 wt.% Si bicrystals[a]

	Samples																
	1	2	3	4	5	6	7	8	9	10	11	12	13	14	15	16	17
φ	0.175	0.210	0.331	0.157	0.140	0.122	0.140	0.594	0.229	0.402	0.052	0.385	0.210	0.367	0.490	0.524	0.280
ψ	0.559	0.052	0.245	0.367	0.332	0.734	0.069	0.210	0.455	0.699	0.052	0.297	0.227	0.455	0.245	0.069	0.542
$(\hat{K})_E$	1.461	1.049	1.168	1.226	1.192	1.575	1.042	1.233	1.283	1.602	1.036	1.225	1.141	1.404	1.204	1.121	1.425
$(\hat{K})_T$	1.465	1.040	1.208	1.301	1.267	1.539	1.045	1.249	1.388	1.563	1.030	1.267	1.171	1.408	1.245	1.116	1.464
$\Delta\hat{K}/(\hat{K})_E$ (%)	0.3	0.9	3.1	5.7	5.9	3.2	0.2	1.2	7.5	2.5	0.6	3.1	2.5	0.3	3.1	0.4	2.6

[a] The subscriptions "E" denotes experimental data; "T" the theoretical results; and $\Delta\hat{K}$ the difference between $(\hat{K})_E$ and $(\hat{K})_T$.

temperature was 350 MPa, leading to an estimate of the effective grain boundary shear strength $k = Y/\sqrt{3}$ around 200 MPa. Thus, we estimate α to be about 3.5, which, according to the river markings shown in Fig. 3, is quite acceptable. In Fig. 8, it can be seen that increasing the twist and tilt misorientations has a beneficial effect on the grain boundary toughness, and the influence of the twist misorientation is more profound. The grain boundary toughness is quite sensitive to the twist misorientation in the middle of its range, which promotes the diversity of the crack front behavior at different grain boundaries.

Since the critical condition of the unstable crack advance across the grain boundary is related to the second derivative of the strain energy, the grain boundary toughness is not a material constant. Instead, with everything else including the crystallographic misorientations the same the value of $\hat{K}$ is higher for longer cracks. However, according to Eq. (19), when a_0 is much larger than w, $\partial\hat{K}/\partial a$ tends to zero, i.e. the crack length dependence becomes negligible. This type of size effect is typical in the R-curve analysis of heterogeneous materials. Eq. (9) shows that G is proportional to a^2 while $\partial G/\partial a$ is linear to a, i.e. the energy release rate rises more rapidly with crack length than $\partial G/\partial a$. Consequently, for a longer crack, since the profile of the R-curve is same, G_{ICGB} must be larger to satisfy the condition of $\partial R/\partial a = \partial G/\partial a$. This size effect can also be attributed to the non-self-similar nature of the crack advance. With the same value of w, the density of BTZ looks "lower" at the tip of a shorter crack, which in turn makes the toughening effect of the grain boundary less significant.

According to Eq. (19), the resistance of the grain boundary to cleavage cracking is strongly influenced by the break-through mode of the crack front. The factor of the spacing between BTZ, w, comes in by affecting the R-curve through two mechanisms. Firstly, the width of BTZ tends to increase with w, which results in higher resistance due to the increase of the work of separation of the grain boundary. Secondly, with increasing w the first derivative of the strain energy decreases more rapidly than the second derivative, thus the resistance of the grain boundary is lowered. The overall effect of increasing w is beneficial to the grain boundary toughness.

The grain boundary toughness also dependents on the profile of the cleavage front prescribed by Eq. (3). The numerical results showed that $\hat{K}$ varied by only about 10% when the value of β was changed by a factor of 2, while the influence of α, which was directly related to the BTZ width, was much more significant. The wider the BTZ, the more grain boundary is involved in the stable crack advance before the critical penetration depth is reached, and, consequently, the higher the grain boundary toughness. The BTZ width should be affected by the fracture mode. In mode-II fracture the cleavage front tends to stretch forward, therefore w_{BT} is relatively small and the toughening effect of the grain boundary is less significant. In mode-III fracture, since the crack front in BTZ tends to expand along the grain boundary, $\hat{K}$ should be relatively high. However, there have not been any experimental data of this phenomenon.

5. Conclusions

In this paper, the penetration process of the cleavage front across high-angle grain boundary was analyzed and the resistance curve associated with the shear deformation along the grain boundary was obtained. When the energy release rate equals the grain boundary resistance the crack starts to stably grow across the grain boundary. With increasing penetration depth more and more grain boundary is involved in the break-through process. The resistance increases continuously while its first derivative with respect to the crack length keeps decreasing. When $\partial R/\partial a = \partial G/\partial a$, the peak resistance of the grain boundary is reached and the crack advance becomes unstable. The following conclusions are drawn:

(1) The grain boundary toughness is dominated by the crystallographic misorientations. The effect of the twist misorientation is more significant than that of the tilt misorientation.
(2) The resistance of the high-angle grain boundary to cleavage cracking is not a material constant. It is more difficult for longer cracks to break through the grain boundary due to the crack length dependence of $\partial G/\partial a$. However, when the crack length is much larger the characteristic microstructure length, this size effect becomes negligible.
(3) The behavior of the cleavage front in BTZ has considerable influence on the grain boundary toughness. The BTZ width was found to be essential. It was predicted that the toughening effect of the grain boundary is more profound in mode-III fracture and less significant in mode-II fracture.

Acknowledgements

The author is grateful to Professor A.S. Argon for the valuable suggestions for understanding the experimental results and Professor E. Pan for the useful discussions of the model.

References

[1] G.T. Hahn, B.L. Averbach, W.S. Owen, M. Cohen, in: Proceedings of the International Conference of Atomic Mechanisms of Fracture, Swampscott, MA, 1959, p. 91.
[2] F.A. McClintock, A.S. Argon, Mechanical Behavior of Materials, CBLS, Marietta, OH, 1993.
[3] D. Padhi, J.J. Lewandowski, Metal. Mater. Trans. A 34A (2003) 967.
[4] D. Hull, Acta Metall. 8 (1960) 11.
[5] R.O. Ritchie, J.F. Knott, J.R. Rice, J. Mech. Phys. Solids 21 (1973) 395.
[6] J.F. Knott, Int. J. Pres. Ves. Pip. 64 (1995) 225.

[7] M. Gell, E. Smith, Acta Metall. 15 (1967) 253.
[8] A. Crocker, G. Smith, P. Flewitt, R. Moskovic, in: Proceedings of the 11th European Conference on Fracture (ECF11), Eng. Mater. Advis. Serv., Warley, UK, 1996, p. 233.
[9] T.L. Anderson, D. Stienstra, R.H. Dodds Jr., in: J.D. Landes, D.E. McCabe, J.A.M. Boulet (Eds.), Fracture Mechanics, vol. 24, ASTM STP-1207, ASTM, Philadelphia, PA, 1994, p. 186.
[10] F.A. McClintock, in: K.S. Chan (Ed.), George R. Irwin Symposium Proceedings on Cleavage Fracture, TMS, Warrendale, PA, 1997, p. 81.
[11] Y. Qiao, A.S. Argon, Mech. Mater. 35 (2003) 313.
[12] A.W. Thompson, J.F. Knott, Metal. Trans. A 24 (1993) 523.
[13] H. Huang, W.W. Gerberich, Acta Metal. Mater. 42 (1994) 639.